Iterative Reconstruction and Statistical Optimization for the Nondestructive Assay of Distributed Gamma Source in a Large Nuclear Waste Container

Chin-Jen Chang and Samim Anghaie

***Abstract*—An iterative reconstruction and statistical optimization method for the nondestructive assay of total source activity of distributed gamma source in a large nuclear waste container is presented. Multiple detectors positioned as closely as possible to the waste barrel are used to measure the emerging radiation field from the distributed radiation source. The source distribution is reconstructed by using the conjugate gradient with nonnegative constraint method or maximum likelihood expectation method based on measured detector responses. Total source activity is estimated by examining the error bond and its associated confidence level. These are determined statistically by performing a large number of numerical experiments involving the counting statistics, the nonuniformity of source distribution, and the heterogeneous density of the self-absorbing medium. Using the conjugate gradient with nonnegative constraint method (CGNN) and maximum likelihood expectation maximum method (MLEM) methods the authors compare results of total activity estimation.**

***Index Terms*— Conjugate gradient, iterative reconstruction, maximum likelihood, nondestructive assay, nuclear waste characterization, statistical optimization.**

I. Introduction

ONE OF THE important tasks for nuclear waste management is the characterization of radioactive sources inside a nuclear waste barrel. Before shipping the nuclear waste barrel to disposal sites, barrel contents need to be determined as high- or low-level waste based on the types and the amount of radionuclides inside. The cost of processing high-level waste is usually far greater than that of low-level waste. Therefore, accurate characterization of the waste barrels is not only environmentally essential but also economically important for the nuclear industry. Most nuclear waste, including commercial power plant waste and defense waste, is stored in cylindrical steel drums (208ℓ waste barrel) about 57 cm in diameter and 88 cm in height [1]. For most applications, using far-field measurement and assuming the drum as a line or a point source are not practical because of the long measurement time associated with the long measurement distance for low-level waste characterization. For a near-field measurement, the estimation error for the total source activity is usually very large because the detection rate is very sensitive to the source distribution and the density of the self-absorbing medium. A practical solution is to implement medical imaging techniques in a near filed measurement, especially the technique of Single Photon Emission Computed Tomography (SPECT) [2]. In these applications, multiple detector positions are used to measure the emerging radiation field. In matrix form, the problem can be represented as follows:

$$D = K \cdot S \tag{1}$$

where D is the vector representing the external detector responses, S is the vector representing the source distribution in the drum, and K is the matrix representing the point response kernel and all the geometrical and physical factors involved in the detection process. The matrix element $K_{i,j}^{(m)}$ corresponds to the uncollided gamma counting rate of the mth energy peak contributed by the jth voxel to the detector at the ith position and is given by

$$K_{i,j}^{(m)} = \exp\left(-\sum_{q\in \mathrm{Ray}(i,j)} \left(\frac{\mu}{\rho}\right)m \cdot \rho_q \cdot t_q\right) \cdot \varepsilon_m \cdot \frac{\Omega_{i,j}}{\Omega_0} \cdot \beta_m \tag{2}$$

where t_q is the path length of the ray (i,j) in the qth voxel; $(\mu/\rho)_m$ is the linear mass attenuation coefficient of the mth gamma energy; ρ_q is the density in the qth voxel; $\Omega_{i,j}$ is the solid angle extended from a source point in the jth voxel to the detector at the ith position; ε_m is the detector efficiency of the mth gamma energy at a calibration position with solid angle Ω_0; and β_m is the branching ratio of the mth gamma energy.

In real implementation, D is measured, K can be calculated based on a known geometric model and detector efficiency, and S can be solved by using a numerical optimization algorithm. Theoretically, if the number of detector responses is equal to the total number of points over which the source is distributed, (1) is well posed and an exact solution can be obtained. However, due to the variability of the source distribution and the heterogeneity of the self-absorbing medium, (1) is either highly undetermined or the matrix K is so ill-conditioned that a unique or stable solution cannot be found [3]. Uncertainties involved in the detection process and choice of solution method can also add to the measurement error.

This paper presents an iterative and statistical optimization method for determining nuclide inventories in a large nuclear waste barrel. Using conventional nondestructive assay methods such as the segmented gamma scanning [4], [5]

Manuscript received July 8, 1997; revised August 26, 1997 and September 16, 1997.

The authors are with the University of Florida, Gainesville, FL 32611-8300 USA.

Publisher Item Identifier S 0018-9499(98)02735-X.

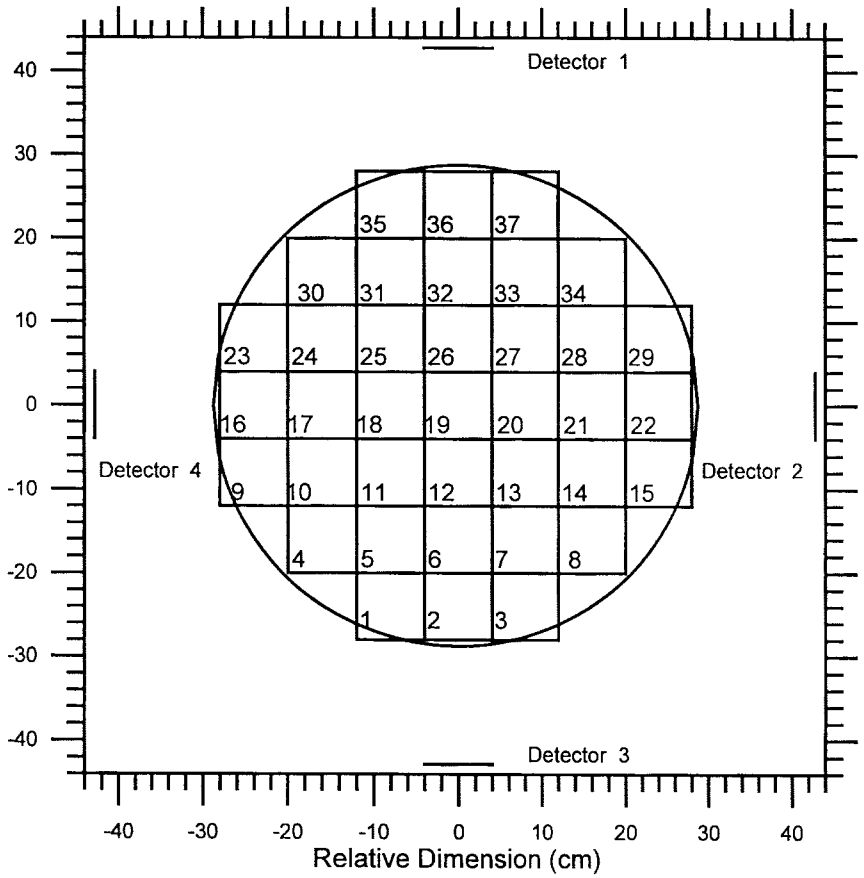

Fig. 1. Configuration of a four-detector positions measuring system in a vertical segment of a 208ℓ nuclear waste barrel.

or the tomographic gamma scanning [6], [7] methods, the measurement accuracy and the associated confidence level cannot be determined. The numerical experiment method, which is described in the next section of this paper, is used to estimate the confidence level for the expected accuracy of the segmented gamma scanning and the tomographic scanning methods. If these methods are to be used for the measurement of the total radionuclide activity in a 208ℓ waste barrel, the confidence level for measurement errors in the order of 50% or less is about 60% [8]–[10]. This uncertainty is below what is considered to be an acceptable upper bound of precision in the nondestructive assay of radioactive nuclear waste barrels. Customarily, it is desirable to achieve measurement precision within 30% of the actual value at 95% confidence level. The 208ℓ waste barrel is studied and each of its vertical segments is modeled to have 37 computational grids (see Fig. 1). If two energy peaks are measured in each of the four detector positions (Fig. 1), (1) is an 8×37 linear system. The source distribution is reconstructed by using the conjugate gradient with nonnegative constraint method (CGNN) [11] or the maximum likelihood expectation maximum method (MLEM) [12], based on measured detector responses. Total source activity is determined by summing the reconstructed activity of each computational grid. The error bound and its associated confidence level of the total activity estimation are determined statistically by performing 10 000 numerical experiments involving of the random source distribution, the counting statistics, and the heterogeneous density of the self-absorbing medium. By examining the statistical results, an optimized estimation of total source activity can be obtained.

II. Conjugate Gradient with Nonnegative Constraint

The conjugate gradient (CG) algorithm is an iterative algebraic solution scheme for solving linear systems of equations and represents an important computational innovation of the early 1950's. This method came into wide use only in the mid-1970's [13], due to the rapid improvement of computer technology. Iterative algebra algorithms, including the CG method and expectation maximum method, have become more and more important in the fields of image reconstruction and remote sensing, which usually require a great deal of matrix operations and computer memory. An application similar to nuclear waste drum characterization is the SPECT for medical imaging in clinical nuclear medicine. SPECT reconstructs images of body organs, which are much smaller than the typical nuclear waste drum. The total activity of nuclear medicine injected into the human body is always known and is usually much larger than the total activity in waste drum characterization, which is usually unknown. Therefore, applying CG in the nuclear waste drum characterization has different considerations from that of SPECT.

From the optimization theorem, the least square solution S of (1) can be found by minimizing the following squared error:

$$e = ||D - K\hat{S}||^2 = (D - K\hat{S})^t(D - K\hat{S}) \qquad (3)$$

where $\|\ \|^2$ means the L^2 norm, $(\ )^t$ means the transpose of the matrix, and $\hat{S}$ means the least square solution of S. In the CG method, solution $\hat{S}$ is found by using an iterative algorithm

$$\hat{S}_{n+1} = \hat{S}_n + \alpha_n d_n \tag{4}$$

where $\hat{S}_n$ is the estimate of $\hat{S}$ at the nth iteration, α_n is a scalar search factor, and d_n is a search vector which is required to be orthogonal to the modified residual vector r_n by the following relation:

$$r_{n+1}^t d_n = 0 \tag{5}$$

with

$$r_n = K^t(D - K\hat{S}_n). \tag{6}$$

Equation (5) means that to approach the minimum point of e, the search vector at a certain iteration step must be orthogonal to the residual vector at the next step. From the relation

$$\begin{aligned}\hat{S}_{n+1} &= \hat{S}_n + \alpha_n d_n \Rightarrow K\hat{S}_{n+1} \\ &= K\hat{S}_n + \alpha_n K d_n \Rightarrow K^t(K\hat{S}_{n+1} - D) \\ &= K^t(K\hat{S}_n - D) + \alpha_n K^t K d_n\end{aligned}$$

and from (6), we get

$$r_{n+1} = r_n - \alpha_n K^t K d_n. \tag{7}$$

To minimize e, we need to take the partial derivative of (3) with respect to α_n and set the result at zero. This leads to

$$\begin{aligned}\frac{\partial(\|D - K\hat{S}\|^2)}{\partial\alpha_n} &= \frac{\partial(\|D - K(\hat{S}_n + \alpha_n d_n)\|^2)}{\partial\alpha_n} \\ &= 0 \Rightarrow \alpha_n = \frac{d_n^t r_n}{d_n^t K^t K d_n}.\end{aligned} \tag{8}$$

The search vector d_n of CG must satisfy the general Gram–Schmidt conjugate properties and is related to the residual vector r through a recursion formula. The conjugate property is

$$d_n^t K^t K d_m = 0, \qquad \text{for } n \neq m \tag{9}$$

and the recursion relation can be derived as

$$d_n = r_n - \beta_{n-1} d_{n-1} \quad \text{or} \quad d_{n+1} = r_{n+1} - \beta_n d_n \tag{10}$$

where β_n is the orthogonality factor.

Taking the inner product of (10) with $K^t K d_{n-1}$ and applying the property of (9), we have

$$\beta_{n-1} = \frac{r_n K^t K d_{n-1}}{d_{n-1}^t K^T K d_{n-1}} \quad \text{or} \quad \beta_n = \frac{r_{n+1} K^t K d_n}{d_n^t K^t K d_n}. \tag{11}$$

The algorithm of CG without constraint is as follows.

Step 1: Set an initial guess of $\hat{S}_1$, and calculate $d_1 = r_1 = K^T(D - K\hat{S}_1)$.

Step 2: Set the loop index starting from $n = 1$, calculate α_n based on (8), calculate $\hat{S}_{n+1}$ based on (4), calculate r_{n+1} based on (7), calculate β_n based on (11), and then calculate d_{n+1} based on (10). The loop ends when a specified criterion of residual difference is reached or a specified iteration number is reached.

The algorithm of CGNN is more complicated than the above algorithm. Suppose there is a hypersurface H that is the boundary of the CGNN solution $\hat{S}_{n+1}$ which minimizes the quadratic function e of (3) and has at least m components which are zero. Then, at $\hat{S}_{n+1}$, any slight increase of component $\hat{S}_{n+1}^m$ at boundary H will increase the e value. Therefore, if I is a set of indexes $i \leq m$ such that $\hat{S}_{n+1}^i = 0$, we have the relations for the optimum point $\hat{S}_{n+1}$ [4]

$$\frac{\partial e}{\partial \hat{S}^i} \geq 0 \quad \text{for } i \text{ in } I \quad \text{and} \quad \frac{\partial e}{\partial \hat{S}^i} = 0 \quad \text{otherwise.}$$

Since the residual is defined as the negative of the gradient value, the criteria for terminating the search and finding a CGNN solution $\hat{S}_{n+1}$ is equivalent to having

$$r_{n+1}^i \leq 0 \quad \text{for } i \text{ in } I \quad \text{and} \quad r_{n+1}^i = 0 \quad \text{otherwise.} \tag{12}$$

A restart algorithm conducts the search method. Within any iteration, if there exists a search vector d_n that will produce negative components of $\hat{S}_{n+1}$, the most negative component is determined, and the scale of the search length is calculated to force this component to be zero. Then, the I set is redefined and the criteria in (12) are checked. If the criteria in (12) are not matched, $\hat{S}_{n+1}$ is reset to be $\hat{S}_1$ and the whole algorithm is restarted.

The most important issue for the CGNN algorithm is the stopping rule termination point. The zero criterion in (12) is customarily set at a very small value which is near to the precision limit of the computer digit. However, because the source activity level covers a very wide range, a fixed value for zero may sometimes stall the algorithm and may also not be an optimal converged point. Zero criterion in (12) for this study is dynamically defined to be a small fraction of the average value of the initial guess of r which is defined in (6). That is

$$\text{ZERO} = \frac{\sum_{m=1}^{37} r_1^m}{37} \cdot \varepsilon \tag{13}$$

where r_1^m is the mth component of initial guess of r and is varied case by case with respect to the measured or calculated detector responses. Table I shows the convergence test on a Pentium/120 computer by studying 10 000 random source distribution cases under homogeneous density condition. A total activity of 10^6 Bq ^{192}Ir is input for every case. Fraction of the total activity is randomly assigned for each computational grid. First, a homogeneous point kernel table comparing matrix elements of K is constructed and detector responses of the measurement system shown in Fig. 1 are calculated by using (1). Then, the source distribution is reconstructed by the CGNN algorithm using four detector positions and two energy peaks of ^{192}Ir. The reconstructed total activity is then

TABLE I
RESULTS OF THE CONVERGENCE TEST FOR DIFFERENT ZERO CRITERIA OF CGNN BY USING 10 000 RANDOM SOURCE DISTRIBUTION CASES OF HOMOGENEOUS DENSITY

ε	Error* <50%	<30%	<25%	<20%	<10%
10^{-1}	4,573	2,957	2,455	2,057	931
10^{-2}	8,356	4,243	3,418	2,555	1,207
10^{-3}	10,000	9,929	9,708	9,213	6,674
10^{-4}	10,000	10,000	10,000	9,993	9,341
10^{-5}	10,000	10,000	10,000	10,000	9,783
10^{-6}	10,000	10,000	10,000	10,000	9,901
10^{-7}	10,000	10,000	10,000	10,000	9,823
10^{-8}	10,000	10,000	10,000	10,000	9,824
10^{-9}	10,000	10,000	10,000	10,000	9,823
10^{-10}	10,000	10,000	10,000	10,000	9,820

compared with the input total activity to determine the percent error for each case. Five categories of percent error are defined as shown in Table I. The cases that fall into a certain category are counted. The value for ε is varied from 10^{-1}–10^{-10}. It is evident that the optimal value of ε among them is 10^{-6}, which predicts 9901 out of 10 000 cases with 10% accuracy.

III. MAXIMUM LIKELIHOOD EXPECTATION MAXIMUM

Maximum likelihood estimation (MLE) is an approach to maximize the likelihood function, which is the probability that the source strength S produces the measured detector responses. As is CG, MLE is an iterative algebraic solution scheme for solving linear systems of equations. It was introduced to emission tomography by Rockmore and Macovski in 1976 [14]. Lange and Carson incorporated the expectation maximum (EM) method in MLE to compute maximum likelihood estimates [11]. MLEM then became popular for application in SPECT methods. It assumes that detector responses are Poisson distributions. Thus, the expectation value of the ith detector response for a waste barrel with 37 computational grids is

$$\overline{D}_i = \sum_{j=1}^{37} K_{ij} S_j = \sum_{j=1}^{37} \overline{X}_{ij} \tag{14}$$

where S_j is the source strength at voxel j and K_{ij} is the probability that a photon leaving voxel j is counted by the ith detector. $\overline{X}_{ij}$ is the expectation value of X_{ij}, which is the statistical number of photons that are emitted from voxel j and contributes to the counts for detector response i. In the MLEM algorithm, a conditional expectation function is defined as

$$E(\ln\ f(X,S)|D,S^{(n)}) \tag{15}$$

where ln denotes the natural logarithm and $S^{(n)}$ is the estimation of S at the nth iteration. This equation defines an expectation function of a logarithm likelihood function $f(X,S)$ under the condition of observed detector response D and source distribution S at the nth iteration step. $f(X,S)$ has the Poisson distribution form of

$$f(X,S) = \prod_{i=1}^{m} \prod_{j=1}^{37} \frac{\overline{X}_{ij}^{X_{ij}} \cdot e^{-\overline{X}_{ij}}}{X_{ij}!} \tag{16}$$

where m is the total number of detector responses. Its logarithm is

$$\begin{aligned} \ln\ f(X,S) &= \sum_i \sum_j (-\overline{X}_{ij} + X_{ij}\ \ln\ \overline{X}_{ij} - \ln\ X_{ij}!) \\ &= \sum_i \sum_j (-K_{ij}S_j + X_{ij}\ \ln(K_{ij}S_j) - \ln\ X_{ij}!). \end{aligned} \tag{17}$$

The conditional expectation of X_{ij} in (17) with respect to D_i and $S^{(n)}$ is

$$N_{ij} = E(X_{ij}|D_i, S^{(n)}) = \frac{K_{ij} S_j^{(n)} \cdot D_i}{\sum_l K_{il} S_l^{(n)}}. \tag{18}$$

Because the third term in (17) has no dependence on the iteration of S, the conditional expectation of (17) becomes

$$\begin{aligned} &E(\ln\ f(X,S)|D,S^{(n)}) \\ &\quad = \sum_i \sum_j [-K_{ij}S_j + N_{ij}\ \ln(K_{ij}S_j)] + C \end{aligned} \tag{19}$$

where C is the term not dependent on the iteration of S. To find the maximum of this expectation, we need

$$\frac{\partial E(\ln\ f(X,S)|D,S^{(n)})}{\partial S_j} = 0 = -\sum_i K_{ij} + \sum_i N_{ij} \frac{1}{S_j}. \tag{20}$$

The partial derivative of the above equation is

$$\frac{\partial^2 E(\ln\ f(X,S)|D,S^{(n)})}{\partial S_j^2} = -\sum_i N_{ij} \frac{1}{S_j^2}. \tag{21}$$

Equation (21) yields a negative value and this assures that $E(\ln\ f(X,S)|D,S^{(n)})$ is a concave function of S and has a maximum at

$$\begin{aligned} S_j^{(n+1)} &= \frac{\sum_i N_{ij}}{\sum_i K_{ij}} = \frac{S_j^{(n)}}{\sum_i K_{ij}} \cdot \sum_i \frac{K_{ij} D_i}{\sum_l K_{il} S_l^{(n)}}, \\ &\qquad i = 1, \cdots, m \\ &\qquad j, l = 1, \cdots, 37. \end{aligned} \tag{22}$$

This iteration algorithm will always assure nonnegative results if the initial guess of the source is positive.

To determine the optimal termination point for the iterative algorithm in (22), the same procedure as described in the CGNN reconstruction is adopted. The termination point is set to be the optimal number of iterations that will give the most satisfactory results from the process of studying 10 000 random source distribution cases. Table II shows the results of the convergence test by varying the iteration number from 100 to 20 000. The optimal prediction among them is 10 000 iterations. MLEM predicts 9350 out of 10 000 cases with

TABLE II
RESULTS OF THE CONVERGENCE TEST FOR DIFFERENT ITERATION NUMBER OF MLEM BY USING 10 000 RANDOM SOURCE DISTRIBUTION CASES OF HOMOGENEOUS DENSITY

It.#	Error* <50%	<30%	<25%	<20%	<10%
100	9,906	6,918	5,832	4,572	2,821
500	10,000	9,963	9,872	9,582	6,547
1,000	10,000	10,000	9,991	9,831	7,800
2,000	10,000	10,000	10,000	9,906	8,573
5,000	10,000	10,000	10,000	9,942	9,122
10,000	10,000	10,000	10,000	9,943	9,350
20,000	10,000	10,000	10,000	9,943	9,163

10% accuracy. The computation time of CGNN using 10 000 iterations and 10^{-6} for the convergence is in the order of 1 min on a Pentium PC computer. The computation time for MLEM using the same number of iteration is about ten times longer than that of the CGNN method.

IV. THE STATISTICAL MODEL

In real experimentation, the computer model uses backward reconstruction algorithms CGNN and/or MLEM to estimate total activity based on observed external detector responses. In numerical experimentation, total activity is obtained from backward reconstruction based on ideal detector responses, which are calculated by a forward projection algorithm using (1). However, the observed responses are always different from calculated ideal responses. These differences are treated as "noise" in this research. To simulate real measurements by using numerical experiments, "noise" is modeled and added to ideal detector responses. Two types of noise are modeled: local nonuniformity noise and counting statistical noise. In addition, a random density perturbation model is used to simulate different types of density heterogeneity and combines these density perturbations with noise perturbations to form a statistical basis of total activity estimation.

Density heterogeneity is modeled by specifying a relative density perturbation level with respect to a homogeneous base density. The Monte Carlo process assigns the perturbed density for each computational grid

$$\rho'_j = \rho^0 \cdot [1 + f \cdot (2\eta_j - 1)] \tag{23}$$

where ρ'_j is the perturbed density for the computational grid j, ρ^0 is the base density, f is the relative density perturbation level, and η_j is the random number generated for the computational grid j. A base density of 1.0 g/cm^3 is used in the simulation. Two relative density perturbation levels, 20% (low) and 50% (high), are studied. Ideal detector responses are generated using the assumption that the source was uniformly distributed within a computational grid. First, a kernel table comprising matrix elements $K_{i,j}^{(m)}$ is constructed. The path length of the uncollided gamma-ray passing each grid is accurately calculated for density perturbation conditions. The matrix element is calculated based on averaging the counting rates (for the mth energy peak at the ith detector position) contributed by the Monte Carlo sampling of 5000 point sources within grid j. Then, a Monte Carlo procedure is used to simulate random distribution of the source within 37 computational grids. A random number generator is used to randomly choose one of 37 grids. A randomly chosen fraction of total source activity is assigned to the randomly selected grid. Then, a second grid is chosen and a randomly selected fraction of the remaining source activity is assigned to this grid. The process continues until all remaining source activity is reduced to a very small value (10^{-4} of original activity). The kernel table is incorporated with the assignment of random source fraction of each grid to give the forward projection of ideal detector responses by using (1).

The calculation model used 37 computational grids for a vertical segment of the waste barrel and assumed that once a source was in a grid, the source was uniformly distributed within that grid. However, it is more likely that the source within a grid is not uniformly distributed. This is an important contributor of noise perturbing the ideal detector response. The local nonuniformity noise is modeled by specifying a relative perturbation level for detector responses. This level is the perturbation range of ideal detector responses, which is assumed to occur in real experiments. A Monte Carlo process is used to select the nonuniformity noise from this range. That is, for each detector position i, the perturbed response (counting rate) is

$$D'_i(E_j) = D^0_i(E_j) \cdot [1 + p \cdot (2 \cdot \eta_i - 1)] \tag{24}$$

where $D'_i(E_j)$ is the perturbed response for energy peak j of detector position i; $D^0_i(E_j)$ is the ideal detector response; p is the relative perturbation level contributed from local nonuniformity noise; and η_i is the random number generated for detector position i. Perturbation levels from 1 to 50% are studied.

Any radiation measurement is subject to the uncertainty of counting statistics. A perturbed detector response $D'_i(E_j)$ calculated from (24) is considered an average value of the measurement of randomly distributed sources nonuniformly distributed inside any computational grid. To simulate a real response with counting statistical behavior, distribution of perturbed detector response $D'_i(E_j)$ is modeled by using a Normal distribution form

$$P(X) = \frac{1}{\sqrt{2\pi} \cdot \sigma} \cdot \exp\left(\frac{-(X - \overline{X})^2}{2\sigma^2}\right) \tag{25}$$

where $\overline{X} = D'_i(E_j), \sigma = \sqrt{D'_i(E_j)/T}$, and T is the counting time. Using the rejection technique, each detector response in the numerical simulation is obtained by sampling from (25), with a sampling range from $\overline{X} - 3\sigma$ to $\overline{X} + 3\sigma$.

Three experimental conditions are studied: 1) homogeneous density and noise-free; 2) heterogeneous with 20% density perturbation and different noise levels; and 3) heterogeneous with 50% density perturbation and different noise levels. For each category, evaluations of error bound and its associated confidence level for activity estimation are carried out by using different backward reconstruction schemes under different simulation conditions. Each simulation is performed

TABLE III
CONFIDENCE LEVELS FOR TOTAL ACTIVITY ESTIMATION BY DIFFERENT OPTIMIZATION ALGORITHMS UNDER THE HOMOGENEOUS AND NOISE-FREE CONDITION

Category (i) : Homogeneous and Noise-Free Condition					
Error	<50%	<30%	<25%	<20%	<10%
HCE1*	0.438	0.301	0.267	0.229	0.120
HME1	0.630	0.372	0.323	0.277	0.158
HCE2	1.000	1.000	1.000	1.000	0.981
HME2	1.000	1.000	1.000	0.994	0.935
HCE3	1.000	1.000	1.000	1.000	0.997
HME3	1.000	1.000	1.000	1.000	0.921

with respect to 10 000 random source distribution cases. The confidence level for the simulation is defined as

$$C = P_r\left(\left|\frac{A_i - A_0}{A_0}\right| \le \varepsilon\right) \tag{26}$$

with A_i being the estimated activity for any single case, A_0 the reference activity, and ε the required accuracy. P_r is the frequency of occurrence for relative error within ε. For example, if the error bound ε is specified as 10%, and 95% of the predicted cases fell within 10% of the actual source strength, the prediction error would be said to be 10% at the 95% confidence level.

A. Homogeneous Density and Noise-Free Condition

Table III shows simulation results of different reconstruction schemes under the homogeneous and noise-free condition. In this simulation category, 1-energy, 2-energy, and 3-energy reconstructions [8] are used for both the CGNN and MLEM algorithms. Confidence levels of 1-energy reconstruction are very low. However, when two energies are used, confidence levels dramatically increase to a very satisfactory result for both CGNN and MLEM reconstructions. All the predictions of the CGNN are within 20% error and the confidence level reaches 98.1% for an accuracy as high as 10%. All the predictions of the MLEM are within 25% error and the confidence level for 10% error is 93.5%. Confidence level increases even more when three energies are used, but not as dramatically as when increasing from one energy to two energies. Almost all the predictions (99.7%) are within 10% error for 3-energy CGNN reconstruction. The confidence level for 10% error is 92.1% for 3-energy MLEM reconstruction. In this simulation condition, prediction ability of the CGNN proved better than that of the MLEM.

B. Heterogeneous Density and Noise-Perturbed Conditions

Table IV shows simulation results for different noise levels under 20% density heterogeneity. Five relative perturbation levels of local nonuniformity (1, 5, 10, 20, and 50%) are simulated. Normal distribution statistics are applied for every noise-perturbed detector response. The results of 1-energy, 2-energy, and 3-energy CGNN and MLEM reconstruction schemes are compared at 5% noise level. It is evident again that the total activity predictions of 1-energy CGNN and MLEM methods are very poor. A surprising finding is that CGNN results slightly deteriorate by changing from a 2-energy to a 3-energy reconstruction scheme. The slight reduction in the confidence level for 3-energy reconstruction case is due to the increase of the numerical error which outweighs the new set of equations for the third energy peak. Confidence levels for 30% accuracy decreases from 96.4 to 93.7%, and for 25% accuracy, decreases from 92.8 to 89.7%. This deterioration phenomenon is not found in the 3-energy MLEM results at this noise level. Table IV also clearly shows influences of noise at this heterogeneity level. For 2-energy CGNN reconstruction, the confidence level for 30% accuracy decreases from 96.9 to 82.1% when the noise level increases from 1 to 50%. For 2-energy MLEM reconstruction, the confidence level for 30% accuracy decreases from 96.8 to 84.0% when the noise level increases from 1 to 50%. Compared with the noise-free cases described in the last paragraph, the performance of the CGNN is reversed with respect to the MLEM in the noisy condition. The CGNN confidence level is degraded faster than that of the MLEM when noise increases. Even in only a 1% noise condition, the MLEM outperforms the CGNN. This phenomenon can be explained by the fact that the MLEM is theoretically based on a statistical derivation and the noise is also modeled statistically by this research. Therefore, the MLEM's performance is somehow more regulative in the noise-perturbed condition. For 50% accuracy, the confidence level is 97.9% for the 2-energy CGNN method and 99.0% for the 2-energy MLEM method. A most likely accuracy for both the CGNN and MLEM methods under 20% heterogeneity

TABLE IV
CONFIDENCE LEVELS FOR TOTAL ACTIVITY ESTIMATION BY DIFFERENT OPTIMIZATION ALGORITHMS UNDER THE 20% HETEROGENEITY AND NOISE-PERTURBED CONDITION

Category (ii): 20% Heterogeneity with Local Nonuniformity and Statistical Noise					
Error	<50%	<30%	<25%	<20%	<10%
C2N01KE2*	0.998	0.969	0.932	0.860	0.563
M2N01KE2	0.998	0.968	0.944	0.877	0.600
C2N05KE1	0.468	0.319	0.278	0.237	0.141
M2N05KE1	0.663	0.395	0.337	0.282	0.160
C2N05KE2	0.998	0.964	0.928	0.857	0.557
M2N05KE2	0.998	0.970	0.944	0.866	0.588
C2N05KE3	0.993	0.937	0.897	0.831	0.553
M2N05KE3	0.999	0.973	0.951	0.894	0.638
C2N10KE2	0.999	0.963	0.919	0.850	0.529
M2N10KE2	0.999	0.968	0.940	0.865	0.573
C2N20KE2	0.998	0.951	0.896	0.805	0.495
M2N20KE2	0.999	0.965	0.912	0.826	0.524
C2N50KE2	0.979	0.821	0.743	0.630	0.314
M2N50KE2	0.990	0.840	0.757	0.639	0.328

TABLE V
CONFIDENCE LEVELS FOR TOTAL ACTIVITY ESTIMATION BY DIFFERENT RECONSTRUCTION ALGORITHMS UNDER THE 50% HETEROGENEITY AND NOISE-PERTURBED CONDITION

Category (iii): 50% Heterogeneity with Local Nonuniformity and Statistical Noise					
Error	<50%	<30%	<25%	<20%	<10%
C5N01KE2*	0.996	0.953	0.922	0.851	0.550
M5N01KE2	0.997	0.953	0.919	0.853	0.585
C5N05KE2	0.998	0.954	0.918	0.844	0.531
M5N05KE2	0.996	0.953	0.916	0.850	0.573
C5N10KE2	0.998	0.955	0.910	0.834	0.515
M5N10KE2	0.996	0.956	0.910	0.840	0.554
C5N20KE2	0.998	0.942	0.892	0.789	0.458
M5N20KE2	0.997	0.951	0.893	0.814	0.498
C5N50KE2	0.978	0.818	0.719	0.605	0.315
M5N50KE2	0.986	0.828	0.738	0.628	0.319
C5N50KE3	0.962	0.786	0.706	0.582	0.296
M5N50KE3	0.986	0.825	0.730	0.636	0.335

condition can be determined from Table IV. It can be defined as the highest accuracy with more than 95% confidence level which can be found from the table. For both 2-energy CGNN and MLEM results shown in Table IV, no confidence level greater than 95% can be found for accuracy higher than 30%. The confidence level for 30% accuracy is 95.1% for the 2-energy CGNN method and 96.5% for the 2-energy MLEM method at 20% noise level. Therefore, the most likely accuracy for both of them is said to be 30% error with a noise level up to 20%.

Table V shows simulation results for different noise levels under 50% density heterogeneity. The results of 2-energy and 3-energy CGNN and MLEM reconstruction schemes are compared at the 50% noise level. Again, results presented in Table V show that for the CGNN, 3-energy reconstruction, the accuracy in the prediction of the total activity does not improve over that of 2-energy reconstruction scheme. The confidence level for 50% accuracy decreases from 97.8 to 96.2%. For 30% accuracy, the confidence level decreases from 81.8 to 78.6%. For the MLEM, the prediction ability of 3-energy reconstruction is comparable to that of 2-energy reconstruction. Confidence levels for 30 and 25% accuracy deteriorate, but for 20 and 10% accuracy, the confidence levels are improved. This means that the overall performance of 3-energy MLEM reconstruction is limited when the noise level is as high as 50%. Therefore, for both CGNN and MLEM application in the high noise condition, the 2-energy reconstruction scheme is the optimal choice. For 50% accuracy, both 2-energy CGNN and 2-energy MLEM reconstruction schemes provide more than a 95% confidence level under a noise level as high as 50%. Using the 2-energy CGNN reconstruction scheme, the most likely accuracy is 30% error with a noise level up to 10%. However, using 2-energy MLEM reconstruction scheme, the most likely accuracy is found to be 30% error with a noise level up to 20%.

C. Total Activity Estimation for the Full Length of the Barrel

All the simulations and analyses presented above emphasized the total activity estimation of a vertical segment of the waste barrel. In the computer model, a vertical segment is 8 cm in height. For the 208ℓ nuclear waste barrel (88 cm in height), a total of 11 segments need to be analyzed. This section presents results of a statistical process to evaluate the most likely accuracy of total activity estimation for the full length of a 208ℓ barrel. It is assured that a vertically restricting collimator is used to limit the field of view of the detector to the axial segment which is under interrogation. Therefore, in this analysis all axial segments are treated independently. In reality, there is no axial collimator that can completely limit the detector's field of view. However, the uncertainty introduced die to the segments' radiation field overlap is not very significant. The detector's field of view spreads in locations which are far from the detector, i.e., on the other side of the barrel. Due to attenuation and flux dilution, the contribution of the radiation sources located in the opposite side of the detector to the overall detection rate is insignificant.

The prediction error of total activity of a vertical segment under a specific density heterogeneity and a noise-perturbed condition is characterized by a relative error distribution function. Statistically, if every segment has the same density heterogeneity and noise-perturbed condition, the same distribution function can be used to estimate the activity for each segment. Total activity for the full length of a barrel is the sum of these segmented activities. To obtain the most likely accuracy of total activity estimation, a Monte Carlo sampling process is performed. First, activity of each vertical segment is assumed to vary in a range from 10^6–10^7 Bq, and it is assigned randomly by using the following relation:

$$ST_m = 10^{(6+\eta_m)}\ \text{Bq} \tag{27}$$

where ST_m is the source activity for the mth vertical segment and η_m is the random number generated for the mth vertical segment. Total activity (ST) of a barrel is

$$ST = \sum_{m=1}^{11} ST_m. \tag{28}$$

Second, activity estimation error for each vertical segment is sampled from a relative error distribution function by using a Monte Carol sampling technique. The estimated activity of each vertical segment is obtained by adding the error to the activity specified for (27). A total activity is summed from the estimated activity of each segment. This estimated total activity is then compared with ST to obtain a total activity estimation error for the full length of a barrel. The above-mentioned process is repeated a total of 10 000 times to define the error bound and its associated confidence level. Another type of vertical activity variation is also studied. The activity of each vertical segment is randomly assigned in the range of 10^5–10^7 Bq by

$$ST_m = 10^{(5+2\cdot\eta_m)}\ \text{Bq}. \tag{29}$$

A similar Monte Carlo sampling process is also used to predict the total activity for the full length of a barrel in this activity range.

Six relative error distribution functions which are generated from the 2-energy CGNN method are used in the Monte Carlo sampling process [8]. Four detector positions at each of 11 axial segments of the barrel are used in the simulation. The density heterogeneity level is 50% and the noise level is set at 5, 20, and 50%, respectively. For the vertical activity variation from 10^6–10^7 Bq and with noise level as high as 50%, the confidence level for the most likely maximum error of 20% is 98.2%, if a detailed density distribution is provided. If only an average density is known, the confidence level for the most likely maximum error of 25% is 96.7%. For the vertical activity variation from 10^5–10^7 Bq and with noise level as high as 50%, the most likely maximum error is 25% at 98.1% confidence level, if the density distribution is known. For this case, if only the average density is known, the most likely maximum error is 30% at 96.5%.

V. Conclusions

In this paper, we presented iterative reconstruction algorithms combining a statistical optimization scheme to determine the most likely value of nuclide inventories in a large waste container. The method introduced is a statistical optimization scheme for determination of the most likely value of total source activity based on a prespecified maximum acceptable error. A numerical experimental model was developed to consider a wide spectrum of measurement conditions, including random source distribution, density heterogeneity, local nonuniformity noise, and counting statistics noise.

The superiority of using multiple energy peaks in reconstruction schemes is evident from the simulations of the homogeneous and noise-free condition which show that both the CGNN and MLEM predict 25% error at 100% confidence level using two or three energy peaks, while they predict 25% error at less than 32.3% confidence level using only one energy peak. In noise-free conditions, 3-energy CGNN reconstruction enhances the prediction ability of 2-energy CGNN reconstruction. However, in noise-perturbed conditions, 3-energy CGNN reconstruction deteriorates the prediction ability of 2-energy CGNN reconstruction. The CGNN confidence level is degraded faster than that of the MLEM when noise increases. Compared with 2-energy MLEM reconstruction, the prediction ability of 3-energy MLEM reconstruction is better at a noise level lower than 50% and becomes worse when the noise level is as high as 50%. For both CGNN and MLEM application in the high noise condition, the 2-energy reconstruction scheme is the optimal choice. Using a four-detector-positions gamma scanning system and measuring multiple energy peaks, the ability of total activity estimation is greatly improved by using the CGNN or MLEM reconstruction algorithm. The approach demonstrated in this research can provide the nuclear industry an accurate and confident method for the nondestructive assay of radionuclide inventory in a large nuclear waste container.

References

[1] D. Reilly, N. Emsslin, H. Smith, Jr., and S. Kreiner, *Passive Nondestructive Assay of Nuclear Materials*, NUREG/CR-5550, United States Nuclear Regulatory Commission, Washington, DC, 1991.

[2] S. Kawata and O. Nalcioglu, "Constrained iterative reconstruction by the conjugate gradient method," *IEEE Trans. Med. Imaging*, vol. MI-4, p. 65, 1985.

[3] H. R. Schwarz, *Numerical Analysis—A Comprehensive Introduction*. New York: Wiley, 1989.

[4] J. K. Sprinkle, Jr., and S. T. Hsue, "Recent advances in segmented gamma scanner analysis," in *Proc. 3rd Int. Conf. Facility Operation-Safeguards Interface*. San Diego, CA: Amer. Nucl. Soc., 1987.

[5] A. Cesana, M. Terrani, and G. Sandrelli, "Gamma activity determination in waste drums for nuclear power plants," *Appl. Radiat. Isot.*, vol. 44, no. 3, p. 517, 1993.

[6] S. Kawasaki, M. Knodo, S. Izumi, and M. Kikuchi, "Radioactivity measurement of drum package waste by a computed-tomography technique," *Appl. Radia. Isot.*, vol. 41, no. 10, p. 983, 1990.

[7] R. J. Estep, T. H. Prettyman, and G. A. Sheppard, "Tomographic gamma scanning to assay heteroheneous radioactive waste," *Nucl. Sci. Eng.*, vol. 118, p. 145, 1994.

[8] C.-J. Chang, "Development of optimized solution methods for inverse radiation transport problems involving the characterization of distributed radionuclides in the large waste container," Ph.D. dissertation, Univ. Florida, 1997.

[9] C.-J. Chang and S. Anghaie, "Non-invasive characterization of radionuclides in a cylindrical container," *Trans. Amer. Nucl. Soc.*, vol. 76, p. 40, 1997.

[10] ——, "On the optimization of nondestructive assay of radionuclide inventory," *Trans. Amer. Nucl. Soc.*, vol. 76, p. 201, 1997.

[11] M. Hestenes, *Conjugate Direction Methods in Optimization*. New York: Springer-Verlag, 1980.

[12] K. Lange and R. Carson, "EM reconstruction algorithms for emission and transmission tomography," *J. Computer Assisted Tomography*, vol. 8, no. 2, p. 306, 1984.

[13] G. H. Golub and D. P. O'Leary, "Some history of the conjugate gradient and lanczos algorithms: 1948–1976," *SIAM Rev.*, vol. 31, no. 1, p. 50, 1989.

[14] A. J. Rockmore and A. Macovski, "A maximum likelihood approach to emission image reconstruction from projection," *IEEE Trans. Nucl. Sci.*, vol. NS-23, p. 1428, 1976.